The Astrophysical Journal, 628:501–513, 2005 July 20


# THE NONPOTENTIALITY OF ACTIVE-REGION CORONAE AND THE DYNAMICS OF THE PHOTOSPHERIC MAGNETIC FIELD

Carolus J. Schrijver, Marc L. DeRosa, Alan M. Title, and Thomas R. Metcalf
Lockheed Martin Advanced Technology Center (ADBS/252), 3251 Hanover Street, Palo Alto, CA 94304;
schryver@lmsal.com, derosa@lmsal.com, title@lmsal.com, metcalf@lmsal.com
*Received 2004 December 15; accepted 2005 March 30*

## ABSTRACT

The magnetic field in the solar photosphere frequently carries strong electric currents, even though the global coronal configuration often resembles a potential field ringed by the heliospheric current sheet. To understand this, we compare *TRACE* EUV images of active-region coronae and potential-field source-surface extrapolations based on *SOHO* MDI magnetograms for 95 active regions. We conclude that significant nonpotentiality of the overall active-region coronal field occurs (1) when new flux has emerged within or very near a region within the last $\sim$30 hr, resulting in complex polarity separation lines, or (2) when rapidly evolving, opposite-polarity concentrations are in contact at $4''$ resolution. If these criteria are met by more than 15% of the region's flux, they correctly identify the (non) potentiality of active-region coronae in 88% of the cases. Flares are found to occur 2.4 times more frequently in active regions with nonpotential coronae than in near-potential regions, while their average X-ray peak flare brightness is 3.3 times higher. We suggest that the currents associated with coronal nonpotentiality have a characteristic growth and decay timescale of $\sim$10–30 hr. We find that shear flows drive enhanced flaring or coronal nonpotentiality only if associated with complex and dynamic flux emergence within the above timescale. We discuss the implications of this finding for the modeling of the coronal-heliospheric coupling.

*Subject headings:* solar wind — Sun: flares — Sun: magnetic fields

*Online material:* javascript animation, enhanced figures

## 1. INTRODUCTION

The magnetic field in the solar corona and its extension into the heliosphere are shaped by the magnetic flux through the solar surface and by electrical currents that may run through the solar atmosphere. Studies of the coupling of the coronal field into the heliosphere suggest that the global coronal magnetic field is often largely potential, provided that high-current systems induced by the pressure of the solar wind plasma are allowed for. The most commonly used model, the potential-field source-surface (PFSS) model, uses this concept to extrapolate the line-of-sight surface magnetic field through the corona and into the heliosphere. When coupled with a solar-wind field advection model, the model solar wind conditions near Earth are frequently found to match the observed conditions quite well during quiescent phases (Schatten et al. 1969; Hoeksema 1984; Zhao & Hoeksema 1995; Wang & Sheeley 1992; Neugebauer et al. 1998; Schrijver & DeRosa 2003).

When observing the innermost corona, in contrast, deviations from potentiality occur frequently: filament configurations, sheared arcades, and—of course—solar flares and coronal mass ejections are all associated with current systems. Often these current systems are substantial enough to cause the coronal magnetic field high above the active regions to be distorted significantly from the potential field configuration. In such cases, the PFSS model does not describe the actual state of the solar coronal field, and thus its mapping of the photospheric field into the heliosphere does not reflect the real corona, so that wind-speed modeling and particle propagation pathways from flare or CME sites to Earth and other locations throughout the heliosphere remain problematic.

What causes such substantial currents? Large currents are found to emerge with active regions and are seen to be induced by the intrusion of emerging flux into preexisting configurations in the photosphere (Leka et al. 1996). Large currents also form in coronal simulations when the surface magnetic field is sheared to study, e.g., the formation of filament configurations. Although theory suggests that such large-current systems are long lived (Melrose 1991), observational studies find them to decay on timescales of only a day or so (e.g., Pevtsov et al. 1994).

In principle, the electrical currents running through the photosphere can be measured by inverting vector-magnetographic data. That process contains multiple stumbling blocks. First, there is the $180^\circ$ ambiguity in direction of the perpendicular component of the vector field. Second, even after resolution of that ambiguity, there is at present no proven tool that reliably extrapolates the photospheric field through the non–force-free layers in the lower atmosphere into the nonlinear force-free field in the coronal volume above the active region. The validation of any such model field extrapolation involves a quantitative comparison with the observed coronal configuration. The measure of nonpotentiality required to match the extrapolated to the observed field configuration should enable comparison of widely different field configurations. However, no such measure has been validated at present. Finally, the coronal images containing traceable loops that lend themselves best to the comparison to field-line extrapolations are the high-resolution *TRACE* EUV coronal images (Handy et al. 1999). These narrowband EUV images show only limited thermal regimes in the coronae of active regions, and these differ from region to region depending on field configuration, evolutionary stage, and size. In light of these issues, establishing the importance of photospheric electrical currents on the coronal field configuration remains out of our reach.

In this study we find that in many cases we can make a *qualitative* assessment of the nonpotentiality of the coronal field by comparing a sampling of field lines of a PFSS extrapolation to the corresponding *TRACE* EUV images of the active regions. This study assesses a sample of 95 active regions, investigating

TABLE 1

SELECTED ACTIVE REGIONS WITH NEARLY POTENTIAL CORONAL FIELDS

| CASE | TIME | $(x, y)$; $(\theta, \phi)$[a] | AR NUMBER | SPOT TYPE[b] | MAGNETIC CLASS[c] | FLARE MAGNITUDES[d] X | M | C | CATEGORY[e] | $f$[f] | NOTE |
|---|---|---|---|---|---|---|---|---|---|---|---|
| 1..... | 1999 Apr 13, 00:05:06 | (0, −300); (−20, 241) | 8512 | Cso | $\beta$-$\gamma$ | ... | ... | 1 | E | 11 | |
| | | | 8513 | Dao | $\beta$-$\gamma$ | | | | | | |
| | | | 8515 | Bxo | $\beta$-$\gamma$ | | | | | | |
| 2..... | 1999 Apr 23, 11:00:00 | (12,−174); (−12, 104) | 8518 | Eao | $\beta$ | ... | ... | ... | D | 11 | |
| 3..... | 1999 Jun 4, 05:58:59 | (169, 245); (14, 282) | 8558 | Dki | $\beta\gamma$ | ... | ... | ... | F | 8 | 4 |
| 4..... | 1999 Jun 16, 12:01:02 | (275, −334); (−17, 127) | 8580 | Cao | $\beta\gamma$ | ... | ... | ... | F | 14 | |
| 5..... | 1999 Jun 27, 13:37:01 | (68, 293); (21, 326) | 8594 | Dai | $\beta$ | ... | 2 | 7, 4, 3, 3, 2, 2 | D | 11 | 2 |
| | | | 8596 | Hsx | $\alpha$ | | | | | | |
| | | | 8598 | Fai | $\beta$-$\gamma$ | | | | | | |
| | | | 8606 | Dai | $\beta\gamma$ | | | | | | |
| 6..... | 1999 Jun 30, 00:00:01 | (130, 255); (17, 298) | 8602 | Dko | $\beta$-$\gamma$ | ... | 1 | 3, 3 | F | 4 | 2 |
| | | | 8609 | Bxo | $\beta$-$\gamma$ | | | | | | |
| 7..... | 1999 Aug 2, 00:00:05 | (−99, 295); (24, 207) | 8650 | Cso | $\beta\gamma$ | ... | ... | 6, 4, 3, 2, 2, 1 | D | [11] | 8 |
| | | | 8651 | Ekc | $\beta$-$\gamma$ | | | | | | |
| 8..... | 1999 Aug 11, 18:00:00 | (130, −321); (−12, 92) | 8662 | Fai | $\beta$-$\gamma$ | ... | ... | 4, 1, 1, 1 | D | 17 | 2 |
| 9..... | 1999 Oct 15, 00:02:59 | (91, 258); (17, 321) | 8728 | Eao | $\beta$ | ... | ... | 1 | E | 4 | 2 |
| | | | 8729 | Ca | $\beta$ | | | | | | |
| 10..... | 1999 Oct 26, 18:59:59 | (77, −352); (−13, 165) | 8739 | Ehi | $\beta$-$\gamma$-$\delta$ | ... | 2, 1 | 6, 3, 3 × 2, 1 | D | [10] | 3 |
| | | | 8743 | Bxo | $\beta$-$\gamma$-$\delta$ | | | | | | |
| 11..... | 1999 Dec 22, 06:28:00 | (−283, 328); (16, 117) | 8806 | Fkc | $\beta$-$\gamma$-$\delta$ | ... | 5, 1, 1 | 3, 3, 4 × 2, 1, 1 | D | 12 | 3, 5 |
| | | | 8807 | Cso | $\beta$-$\gamma$-$\delta$ | | | | | | |
| 12..... | 1999 Dec 30, 00:01:01 | (−127, 521); (27, 26) | 8810 | Fko | $\beta\gamma$-$\delta$ | ... | ... | 1 | E | 4 | 4 |
| 13..... | 2000 Mar 10, 00:50:00 | (341, −102); (−10, 198) | 8898 | Eko | $\beta\gamma$ | ... | ... | ... | D | 12 | |
| | | | 8903 | Cro | $\beta\gamma$ | | | | | | |
| 14..... | 2000 Mar 26, 09:10:00 | (−13, −171); (−14, 323) | 8921 | Dai | $\beta$ | ... | ... | 7 | F | 6 | 4 |
| 15..... | 2000 May 7, 21:37:00 | (−290, 473); (27, 101) | 8983 | Cso | $\beta$ | ... | ... | ... | E | [5] | 5 |
| 16..... | 2000 May 31, 01:26:59 | (−35, −211); (−12, 173) | 9017 | Fko | $\beta$-$\gamma$ | ... | ... | ... | D | 10 | |
| 17..... | 2000 Jun 29, 10:00:00 | (303, 147); (10, 166) | 9055 | Hsx | $\alpha\gamma$ | ... | ... | ... | E | 7 | |
| | | | 9057 | Cso | $\beta\gamma$ | | | | | | |
| 18..... | 2000 Jul 1, 17:00:02 | (17, −276); (−12, 118) | 9061 | Hsx | $\alpha\gamma$ | ... | ... | ... | E | 2 | |
| | | | 9062 | Dki | $\beta$ | | | | | | |
| 19..... | 2000 Sep 4, 20:05:01 | (332, 100); (10, 356) | 9147 | Cao | $\beta$ | ... | ... | 3, 3 × 2, 1, 1 | D | 10 | 2 |
| | | | 9149 | Eai | $\beta$ | | | | | | |
| | | | 9151 | Bxo | $\beta$ | | | | | | |
| 20..... | 2000 Jan 13, 12:00:11 | (295, −323); (−12, 203) | 9188 | Dso | $\beta\gamma$ | ... | ... | ... | E | 0 | |
| | | | 9192 | Dso | $\beta\gamma$ | | | | | | |
| 21..... | 2001 Mar 15, 00:00:01 | (−67, −118); (−11, 332) | 9373 | Fsi | $\beta$-$\gamma$ | ... | ... | 2, 1 | G | 10 | 2 |
| | | | 9374 | Axx | $\alpha\gamma$ | | | | | | |
| 22..... | 2003 Mar 13, 00:00:00 | (−196, 262); (7, 75) | 10306 | Dko | $\beta\gamma$ | ... | ... | ... | E | 9 | 2 |
| | | | 10308 | Hrx | $\alpha\gamma$ | | | | | | |

NOTES.—(1) Smaller emerging region next to main region. (2) Multiple small-scale flux emergences and cancellations. (3) Substantial shear and polarity confusion in neutral zone, with relatively compact flux emergence and cancellation. (4) Some sites of cancellation of relatively small patches of flux. (5) Limited, compact (late or new) emergence of flux. (6) Eight C- and B-class flares listed on 1999 August 16 and 17. (7) As 3, but ended no more than ~30 hr from listed time. (8) Leading spot contains most of the leading flux of the main regions in the field of view. (9) Strongly sheared displacements and rapid cancellation near neutral line. (10) As 3, but within the one of the polarity plages. (11) Substantial cancellation of touching polarities along a main neutral line.

[a] Distance to disk center (arcseconds); Carrington longitude and latitude (degrees).

[b] Spot classification consists of three letters. The first character describes the group complexity: (A) single small spot; (B) very small distrib. of small spots; (C) two or more small spots, at least one with penumbra; (D) moderately sized group; (E) moderate to large area of fair complexity with several spots with penumbrae; (F) large to very large area of a complex system; (H) single large spot. The second character describes the penumbra of the largest spot: (x) single spot; (r) rudimentary; (s) small symmetric; (a) small asymmetric; (h) large symmetric; (k) large asymmetric. The third character describes the group compactness: (x) single spot; (o) open; (i) intermediate; (c) compact.

[c] Magnetic Class: ($\alpha$) single-polarity spot; ($\beta$) bipolar spot configuration; ($\gamma$) atypical mixture of polarities; ($\beta\gamma$) mixture of polarities in a dominantly bipolar configuration; ($\delta$) opposite polarity umbrae within single penumbra; ($\beta\delta$) $\beta$ with a $\delta$ configuration; ($\beta\gamma\delta$) $\beta\gamma$ with a $\delta$ configuration.

[d] X-, M-, and C-class X-ray flares for all regions within the field of view between 48 hr before and 24 hr after the listed time, identified by their integer magnitudes within the class.

[e] Categories A–G as described in § 4.4.

[f] Estimated maximum absolute flux that meets criteria A–D (§ 4.4) relative to the total flux; between brackets if very uncertain.

TABLE 2

SELECTED ACTIVE REGIONS WITH SIGNIFICANTLY NONPOTENTIAL CORONAL FIELDS

| CASE | TIME | $(x, y)$; $(\theta, \phi)$[a] | AR NUMBER | Spot TYPE[b] | MAGNETIC CLASS[c] | FLARE MAGNITUDES[d] | | | CATEGORY[e] | $f$[f] | NOTE |
|---|---|---|---|---|---|---|---|---|---|---|---|
| | | | | | | X | M | C | | | |
| 23..... | 1999 May 30, 06:00:00 | (8, 387); (21, 338) | 8552 | Dai | $\beta\gamma$ | ... | ... | ... | A | 28 | 9 |
| | | | 8559 | Dko | $\beta\gamma$ | | | | | | |
| | | | 8561 | Axx | $\alpha\gamma$ | | | | | | |
| 24..... | 1999 Jul 2, 06:00:00 | (−32, −442); (−23, 257) | 8611 | Fai | $\beta\gamma$ | ... | 1 | 8, 3 × 3, 2 | AB | 31 | 3 |
| 25..... | 1999 Aug 20, 07:17:30 | (78, 249); (18, 336) | 8668 | Dko | $\beta$ | ... | ... | ... | ... | ... | 6, 8 |
| 26..... | 1999 Sep 15, 00:58:00 | (204, 232); (22, 365) | 8693 | Cso | $\beta\gamma$ | ... | ... | 4, 2, 1, 1 | A | 34 | 3 |
| | | | 8699 | Eai | $\beta\gamma$ | | | | | | |
| 27..... | 1999 Jan 9, 06:01:01 | (72, 165); (13, 36) | 8716 | Cso | $\beta\gamma$ | ... | ... | 6, 2, 2, 1, 1 | A | 19 | 9 |
| | | | 8720 | Bxo | $\beta$ | | | | | | |
| 28..... | 2000 Apr 11, 08:10:00 | (264, −156); (−13, 128) | 8948 | Eai | $\beta\gamma\delta$ | ... | 3, 3 × 1 | 8, 8, 5, 3 × 2, 3 × 1 | AB | 47 | 3 |
| | | | 8957 | Dao | $\beta\gamma\delta$ | | | | | | |
| 29..... | 2000 May 20, 05:04:00 | (−146, 284); (13, 310) | 9002 | Fkc | $\beta\gamma$ | ... | 2 | 8, 7, 6, 5, 4, 3, 3 × 2 | B | 34 | 3 |
| 30..... | 2000 Jun 8, 00:37:59 | (105, 357); (19, 77) | 9026 | Fkc | $\beta\gamma\delta$ | 2, 1, 1 | 7, 2 | 7 × 2, 3 × 1 | AB | 21 | 9 |
| | | | 9030 | Axx | $\alpha\gamma\delta$ | | | | | | |
| 31..... | 2000 Jun 13, 00:57:00 | (263, 358); (23, 21) | 9033 | Fki | $\beta\gamma$ | ... | ... | 3, 2 | AC | 41 | 10 |
| | | | 9041 | Dao | $\beta\gamma$ | | | | | | |
| 32..... | 2000 Jun 21, 12:49:50 | (14, 307); (20, 252) | 9046 | Dhi | $\beta\gamma$ | ... | ... | 4, 1, 1 | ... | ... | 11 |
| | | | 9051 | Axx | $\alpha\gamma$ | | | | | | |
| 33..... | 2000 Jul 8, 00:00:01 | (−40, 236); (18, 31) | 9070 | Eao | $\beta\gamma$ | ... | ... | 6, 5, 5, 4, 3, 3 × 2, 1 | A | 50 | 3 |
| 34..... | 2000 Jul 14, 00:55:00 | (−52, 240); (19, 310) | 9077 | Fkc | $\beta\gamma\delta$ | 5, 1 | 5, 3, 1, 1 | 5, 5, 4 | B | 34 | 9 |
| 35..... | 2000 Jul 21, 01:43:00 | (139, −206); (−6, 229) | 9087 | Fkc | $\gamma\delta\delta$ | ... | 6, 5, 3, 1 | 9, 7, 7, 6, 6, 4, 3, 3 | AC | 29 | 9 |
| 36..... | 2000 Aug 8, 06:01:01 | (−187, 111); (10, 328) | 9114 | Eai | $\beta\gamma$ | ... | ... | 2, 1 | AB | 23 | 3 |
| 37..... | 2000 Sep 24, 18:02:01 | (134, 45); (7, 81) | 9167 | Cso | $\beta$ | ... | ... | 8, 5, 3 × 2 | AB | 14 | 11 |
| | | | 9169 | Fkc | $\beta\gamma\delta$ | | | | | | |
| | | | 9170 | Dao | $\beta\gamma\delta$ | | | | | | |
| 38..... | 2000 Oct 22, 20:22:00 | (23, 175); (12, 63) | 9204 | Axx | $\alpha\gamma$ | ... | 3 | 2, 2, 1 | A | 17 | 3 |
| | | | 9201 | Dai | $\beta\gamma$ | | | | | | |
| 39..... | 2000 Nov 4, 05:01:02 | (−31, 177); (11, 257) | 9218 | Dao | $\beta\gamma$ | ... | ... | 5, 5, 3, 2, 2 | A | 30 | 7 |
| | | | 9212 | Dso | $\beta$ | | | | | | |
| 40..... | 2000 Nov 18, 14:50:00 | (−172, −440); (−23, 57) | 9231 | Fai | $\beta\gamma$ | ... | 1 | 2, 2, 5×1 | AC | 18 | 2 |
| 41..... | 2000 Nov 28, 10:19:59 | (−22, 178); (8, 298) | 9240 | Cao | $\beta\gamma$ | ... | ... | ... | ... | ... | 8 |
| 42..... | 2001 Jan 24, 02:40:00 | (−9, −17); (−5, 272) | 9313 | Cao | $\beta\gamma$ | ... | ... | 2 | AB | 61 | |
| | | | 9316 | Cao | $\beta\gamma$ | | | | | | |
| 43..... | 2003 Jul 13, 00:00:00 | (287, −210); (−7, 292) | 10401 | Dao | $\beta$ | ... | ... | 2, 1 | B | [29] | 7 |
| | | | 10404 | Axx | $\alpha$ | | | | | | |
| | | | 10406 | Cao | $\beta$ | | | | | | |

NOTES.—(Same as for Table 1.) (1) Smaller emerging region next to main region. (2) Multiple small-scale flux emergences and cancellations. (3) Substantial shear and polarity confusion in neutral zone, with relatively compact flux emergence and cancellation. (4) Some sites of cancellation of relatively small patches of flux. (5) Limited, compact (late or new) emergence of flux. (6) Eight C- and B-class flares listed on 1999 August 16 and 17. (7) As 3, but ended no more than ~30 hr from listed time. (8) Leading spot contains most of the leading flux of the main regions in the field of view. (9) Strongly sheared displacements and rapid cancellation near neutral line. (10) As 3, but within the one of the polarity plages. (11) Substantial cancellation of touching polarities along a main neutral line.

[a] Distance to disk center (arcseconds); Carrington longitude and latitude (degrees).

[b] Spot classification consists of three letters. The first character describes the group complexity: (A) single small spot; (B) very small distrib. of small spots; (C) two or more small spots, at least one with penumbra; (D) moderately sized group; (E) moderate to large area of fair complexity with several spots with penumbrae; (F) large to very large area of a complex system; (H) single large spot. The second character describes the penumbra of the largest spot: (x) single spot; (r) rudimentary; (s) small symmetric; (a) small asymmetric; (h) large symmetric; (k) large asymmetric. The third character describes the group compactness: (x) single spot; (o) open; (i) intermediate; (c) compact.

[c] Magnetic Class: ($\alpha$) single-polarity spot; ($\beta$) bipolar spot configuration; ($\gamma$) atypical mixture of polarities; ($\beta\gamma$) mixture of polarities in a dominantly bipolar configuration; ($\delta$) opposite polarity umbrae within single penumbra; ($\beta\delta$) $\beta$ with a $\delta$ configuration; ($\beta\gamma\delta$) $\beta\gamma$ with a $\delta$ configuration.

[d] X-, M-, and C-class X-ray flares for all regions within the fov between 48 h before and 24 hr after the listed time, identified by their integer magnitudes within the class.

[e] Categories A–G as described in § 4.4.

[f] Estimated maximum absolute flux that meets criteria A–D (§ 4.4) relative to the total flux; between brackets if very uncertain.

TABLE 3
SELECTED ACTIVE REGIONS WITH AMBIGUOUS CORONAL FIELDS

| CASE | TIME | $(x, y)$; $(\theta, \phi)$[a] | AR NUMBER | SPOT TYPE[b] | MAGNETIC CLASS[c] | FLARE MAGNITUDES[d] X | M | C | CATEGORY[e] | $f$[f] | NOTE |
|---|---|---|---|---|---|---|---|---|---|---|---|
| 44..... | 1999 Apr 10, 03:49:00 | (47, 449); (20, 282) | 8508 | Dai | $\beta$-$\gamma$-$\delta$ | ... | 1 | 6, 3, 3, 2, 2, 4 × 1 | A | 14 | 3 |
| | | | 8509 | Bxo | $\beta$-$\gamma$-$\delta$ | | | | | | |
| 45..... | 1999 May 7, 14:15:02 | (311, 353); (15, 295) | 8525 | Cso | $\beta\gamma$ | ... | ... | 7, 2, 1 | A | 7 | 1 |
| | | | 8527 | Axx | $\alpha\gamma$ | | | | | | |
| | | | 8538 | Cro | $\beta\gamma$ | | | | | | |
| 46..... | 2000 May 5, 03:10:01 | (22, 434); (20, 196) | 8939 | Cso | $\beta$-$\gamma$ | ... | ... | ... | B | 10 | 3 |
| | | | 8940 | Hsx | $\alpha\gamma$ | | | | | | |
| 47..... | 2000 Jul 25, 16:14:00 | (170, 53); (5, 168) | 9096 | Dso | $\beta\gamma$ | ... | 8, 1 | 4, 3, 2, 2 | AB | 20 | 11 |
| | | | 9097 | Ekc | -$\gamma$ | | | | | | |

NOTES.—(Same as for Table 1.) (1) Smaller emerging region next to main region. (2) Multiple small-scale flux emergences and cancellations. (3) Substantial shear and polarity confusion in neutral zone, with relatively compact flux emergence and cancellation. (4) Some sites of cancellation of relatively small patches of flux. (5) Limited, compact (late or new) emergence of flux. (6) Eight C- and B-class flares listed on 1999 August 16 and 17. (7) As 3, but ended no more than ~30 hr from listed time. (8) Leading spot contains most of the leading flux of the main regions in the field of view. (9) Strongly sheared displacements and rapid cancellation near neutral line. (10) As 3, but within the one of the polarity plages. (11) Substantial cancellation of touching polarities along a main neutral line.

[a] Distance to disk center (arcseconds); Carrington longitude and latitude (degrees).

[b] Spot classification consists of three letters. The first character describes the group complexity: (A) single small spot; (B) very small distrib. of small spots; (C) two or more small spots, at least one with penumbra; (D) moderately sized group; (E) moderate to large area of fair complexity with several spots with penumbrae; (F) large to very large area of a complex system; (H) single large spot. The second character describes the penumbra of the largest spot: (x) single spot; (r) rudimentary; (s) small symmetric; (a) small asymmetric; (h) large symmetric; (k) large asymmetric. The third character describes the group compactness: (x) single spot; (o) open; (i) intermediate; (c) compact.

[c] Magnetic Class: ($\alpha$) single-polarity spot; ($\beta$) bipolar spot configuration; ($\gamma$) atypical mixture of polarities; ($\beta\gamma$) mixture of polarities in a dominantly bipolar configuration; ($\delta$) opposite polarity umbrae within single penumbra; ($\beta\delta$) $\beta$ with a $\delta$ configuration; ($\beta\gamma\delta$) $\beta\gamma$ with a $\delta$ configuration.

[d] X, M, and C-class X-ray flares for all regions within the fov between 48 h before and 24 hr after the listed time, identified by their integer magnitudes within the class.

[e] Categories A–G as described in § 4.4.

[f] Estimated maximum absolute flux that meets criteria A–D (§ 4.4) relative to the total flux; between brackets if very uncertain.

which photospheric properties contribute most strongly to any nonpotentiality of the coronal field over active regions.

As we cannot yet provide a quantitative measure for the goodness of fit of the model potential field to the observed corona, we analyze those active regions with coronae that are either good matches to potential field models or, in contrast, that exhibit obvious deviations throughout much of their overlying coronal volume. We then compare the magnetic properties of these two classes of regions in order to learn how "near-potential" and "nonpotential" coronae can be differentiated.

We stress that this nomenclature refers only to the compatibility of the PFSS extrapolation with the observed coronae. Currents are expected to run throughout the corona because of the evolution of the surface field subject to, for example, the footpoint braiding by the granulation. These are likely a mixture of oppositely directed currents with little impact on the overall coronal geometry. Weak distributed currents may also exist. In this study, however, we focus on those large currents that affect the entire active-region field configuration, irrespective of whether they run as extended diffuse currents throughout the active-region coronal field or—more likely—in compact regions of the low corona, chromosphere, or photosphere.

## 2. MAGNETIC DATA AND FIELD MODEL

The lower boundary condition used in our PFSS model is a set of full-sphere magnetic maps for the entire mission period of *TRACE* (1998 April through the present). These maps are generated by a field-assimilation code (Schrijver & DeRosa 2003) that inserts the magnetic fluxes within 55° of disk center from available full-disk *SOHO* MDI magnetograms (Scherrer et al. 1995), yielding the magnetic flux on the photosphere at ~6 hr intervals. This flux, partitioned into flux concentrations, is evolved in time subject to models for differential rotation, meridional advection, and supergranular random walk. For each 6 hr time step, we compute the coronal field using the PFSS model (Schrijver & DeRosa 2003).

We also generate movies of the magnetic field over 4 day intervals for each of the selected regions (see § 3). To that end, MDI full-disk magnetograms are selected at the standard 96 minute cadence starting 72 hr prior to the times listed in Tables 1, 2, and 3. These magnetograms are remapped to the perspective corresponding to the tabulated times using approximate scales and target locations applying an average solid-body rotation rate for the center of the *TRACE* field of view. Snapshots for the magnetograms nearest to these times are shown in Figures 1 and 2.

## 3. SELECTION OF OBSERVATIONAL DATA

We start from a database[1] of comparisons of *TRACE* EUV images to PFSS model fields for the entire *TRACE* mission (Handy et al. 1999), which started regular operations around the middle of 1998 April. For each explicit *TRACE* pointing command, we identify Fe IX/X 171 Å (~1 MK) or, if not available, Fe XII 195 Å (~1.5 MK) images taken within 1 hr of the implementation of the instructed pointing. Preference is given to the full field of view of 1024 × 1024 pixels, with 768 × 768 pixel fields of view accepted as alternatives.

For all *TRACE* images that meet these criteria, we identify the surface magnetic field map described in § 2 within 3 hours of the *TRACE* observation. We trace 200 field lines, starting from the photosphere, with starting positions selected at random within the *TRACE* field of view, weighting the selection probability with the absolute magnetic flux density. A second set of 200 field lines is computed with photospheric starting positions distributed uniformly within the field of view. Together,

[1] See http://www.lmsal.com/forecast/TRACEview.

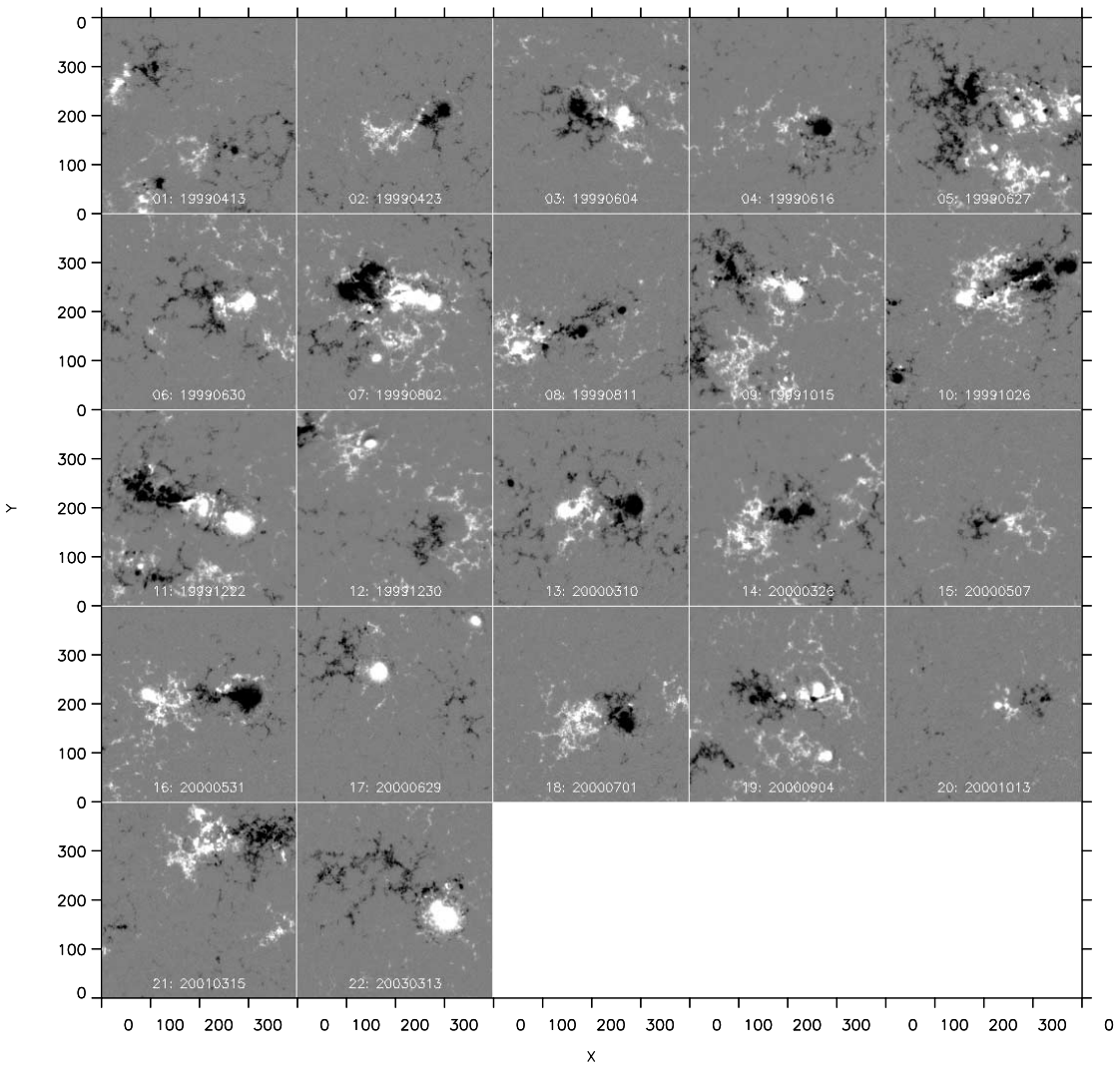


FIG. 1.—*SOHO* MDI magnetograms for 22 *TRACE* pointings, listed in Table 1, for regions for which the coronal field is largely potential. Each panel shows a magnetogram area of 400″ square and is identified by the number as in Tables 1 and 2 followed by the date (yyyymmdd). Solar north is up, east to the right.

these two sets adequately represent both the compact high flux density regions and the extended weak-field regions.

These field lines are projected onto the *TRACE* images, showing all field lines from the first set and only those field lines from the second set that are open to the heliosphere. Examples of these overlays are shown in Figures 3 and 4 for two cases each from Tables 1 and 2, respectively; the complete set of overlays is available in a tar file with the electronic edition. The high-contrast H$\alpha$ images nearest in time from the Big Bear Solar Observatory on-line archive are shown for comparison purposes in the summary composite images 3 and 4 in the electronic edition.

Active regions within a 480″ square region centered on the pointing are identified from the NOAA active-region summary data. The characteristics of the spots and of the field configurations of these regions are summarized in Tables 1 and 2.

From this sample of *TRACE* pointings, we selected pointings from the spring of 1999 through early 2001 (characteristic of cycle maximum) and some in 2003 (descending phase of the cycle) for which *TRACE* followed the active region(s) for at least 5 days, that were well within the flux-assimilation window set to 55° from disk center, and for which full-disk *SOHO* MDI magnetograms are available at at least 6 hr intervals for the entire time *TRACE* pointed at the region. The regions chosen for this study all are significantly larger than the PFSS-model resolution of 1°, and all have a substantial set of loops evident in either the *TRACE* 171 or 195 Å image. We separate regions for which the field lines from the PFSS model agreed well (Table 1) with the observed coronal loops from those with poor agreement (Table 2), listing ambiguous cases in Table 3.[2]

The assessment of whether we label the observed emission patterns as a near-potential or nonpotential region is based on a visual inspection of the overlays of the model field lines on the *TRACE* EUV image, such as the examples shown in Figures 3 and 4. We give particular weight to (1) the correspondence of the directional patterns of field lines with long loops in the outer perimeter of the active-region corona and those emanating from the sunspots and (2) the correspondence of topological features such as (quasi-)separatrices (where loop and field-line connectivity change markedly) and coronal null-point configurations (with X-point signatures), and to the matching of EUV-dark regions to

[2] The 4 day MDI movies and the full-resolution overlays of the potential field lines on the selected *TRACE* 171 or 195 Å images, as well as the correlation diagrams summarized in § 4.1, are available as a tar package that can be accessed either at the electronic version of this paper or at http://www.lmsal.com/~schryver/ARcoronae (500 MB uncompressed).

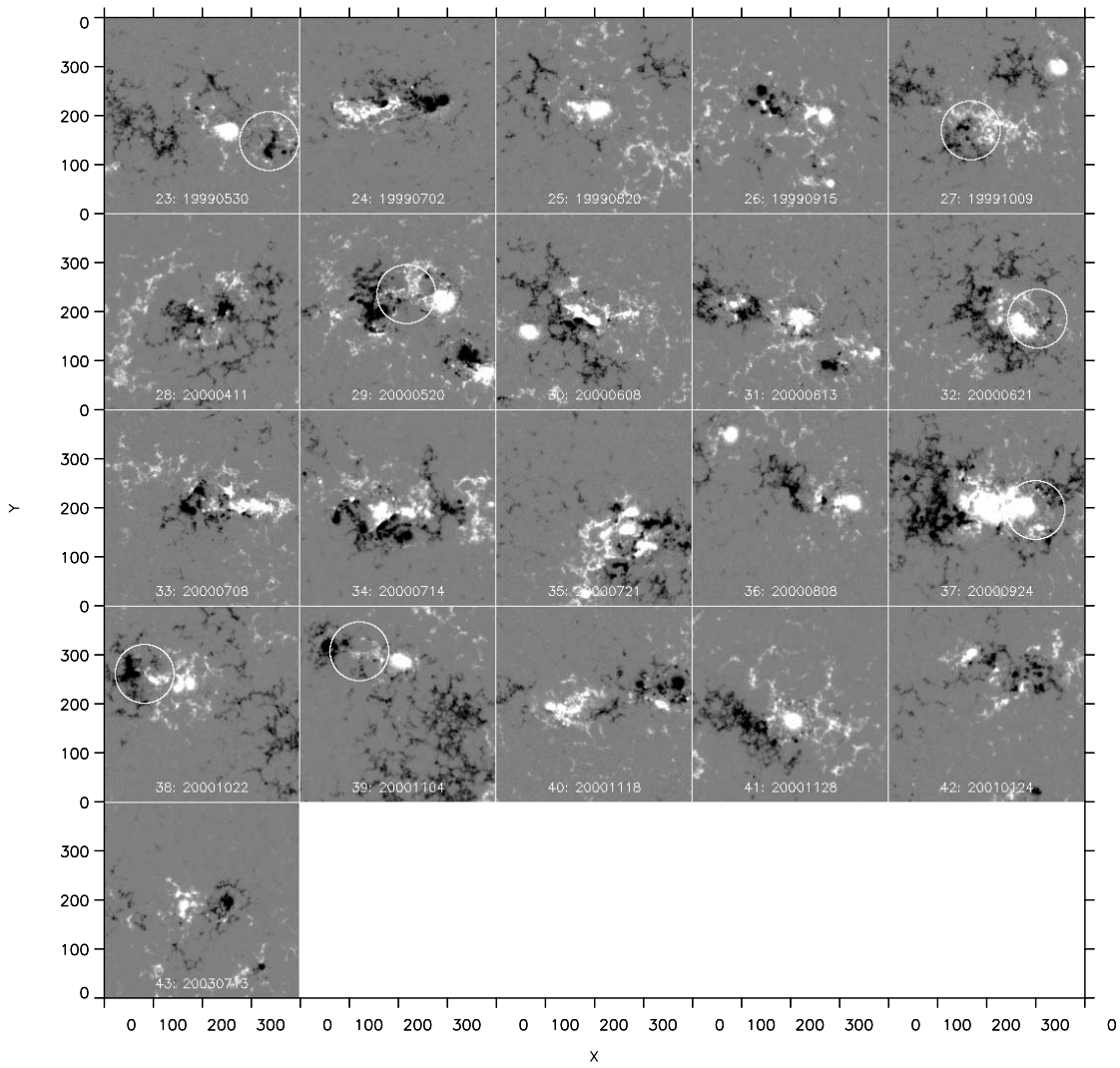


FIG. 2.—As Fig. 1, but for the 21 regions in Table 2 for which the coronal field appears significantly nonpotential. The circles identify special cases described in § 4.4.

model field lines that are open to the heliosphere (shown as colored lines in the electronic version of the Journal). We give little weight to low-lying or short loops, in part because the focus of this study is the appearance of the large-scale active-region corona in relation to the coupling into the heliosphere, and in part because the $1^\circ$ resolution of the spherical harmonics used for the PFSS model does not allow the proper representation of short loops.

The examples in Figures 3 and 4 illustrate how these criteria and weighting result in our sorting: case 16 shows a good correspondence with the loop fan emanating from the leading sunspot, a fair correspondence with the loops in the northern part of the active region, and a good mapping of the separator in the trailing polarity. Case 19 is less clear cut, but shows a fairly good correspondence for the loops from the leading polarity, a rough correspondence of open field with a dark patch on the right, a coronal null where field lines show one near $(x,\ y) = (250,\ 150)$, and there is some correspondence for the separator structure in the trailing polarity. Case 24, in contrast, shows very obvious difference between loops and field lines for all loops in the northern, top half of the image, and a clear deviation for the separator structure in the lower left part of the region. Case 39 shows a complete lack of correspondence for the western, right-hand side of the image, as well as for the fan of moderately long loops coming for the field concentration centered at $(x,\ y) = (160,\ 240)$. In general, it is true that clearly nonpotential cases deviate very strongly from the PFSS model for much of the *TRACE* images, whereas the regions classified as near-potential often show some regions where deviations are relatively strong even as the rest of the images shows a fair or good match. Our term "near-potential" should consequently not be taken to imply that the entire active-region coronae are truly close to a potential field on large scales.

The visual assessment of regions as "near-potential" or "nonpotential" is clearly subjective, depending on what regions of the observed area are weighted most. In order to mitigate personal biases, a randomly ordered set of overlays such as shown in Figures 3 and 4 was provided to three of the authors for classification. Their classifications were unanimous for 43 out of the 47 fields of view, as listed in Tables 1 and 2. The four remaining cases are listed in Table 3 and discussed further at the end of § 4.

## 4. DISCUSSION

In this section, we study the complexity and evolution of the photospheric field and demonstrate that the large-scale measures of cross- and auto-correlation coefficients (§§ 4.1–4.3) are not useful as differentiators between near-potential and nonpotential

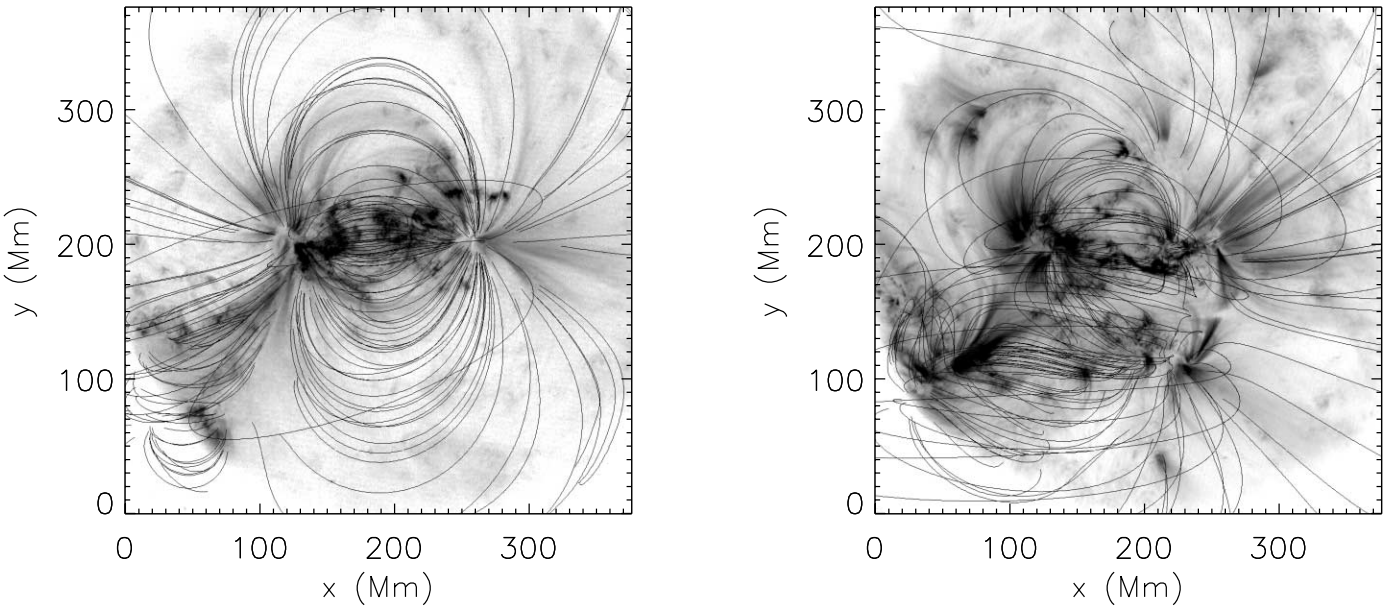


FIG. 3.—Representative *TRACE* EUV images (*negative gray scale*) with field-line overlays for the near-potential cases 16 and 19 listed in Table 1. Color versions of such overlays for all cases studied here and a javascript animation are available in the electronic edition of the Journal.

active-region coronal fields. Evolutionary characteristics of the magnetic field, in contrast, can be usefully applied for that purpose (§ 4.4).

### 4.1. *Overall Field Properties*

What differentiates the near-potential cases in Table 1 from the clearly nonpotential cases in Table 2? Traditional descriptors of active regions or their spots are clearly not significant differentiators: whereas there are more *c*- and $\delta$-type regions in the nonpotential category, the overall distributions of these magnetic characteristics are not useful as differentiators between regions with near-potential and nonpotential coronal fields.

Other measures for the overall pattern or evolution of the magnetic field also do not serve as useful discriminators for the degree of potentiality. For example, Figure 5 compares temporal and spatial correlation properties of the magnetogram sequences for all selected regions. These scatter diagrams compare the cross-correlation coefficients for 0.5 (*left*) and 1.0 day (*right*) temporal lags to the characteristic length scale here defined as the average *e*-folding distance for the auto-correlation functions in the east-west and north-south directions. There is a clear tendency for regions with a larger characteristic length scale to decorrelate more slowly, not surprisingly, but the near-potential cases (*diamonds*) and nonpotential cases ( *plus symbols*) are not differentiated by these global measures.

Tables 1 and 2 suggest that the nonpotentiality involves the rapidly evolving strong-field regions related to flaring (see § 4.2). Flares often occur within the strong-field region of plages,

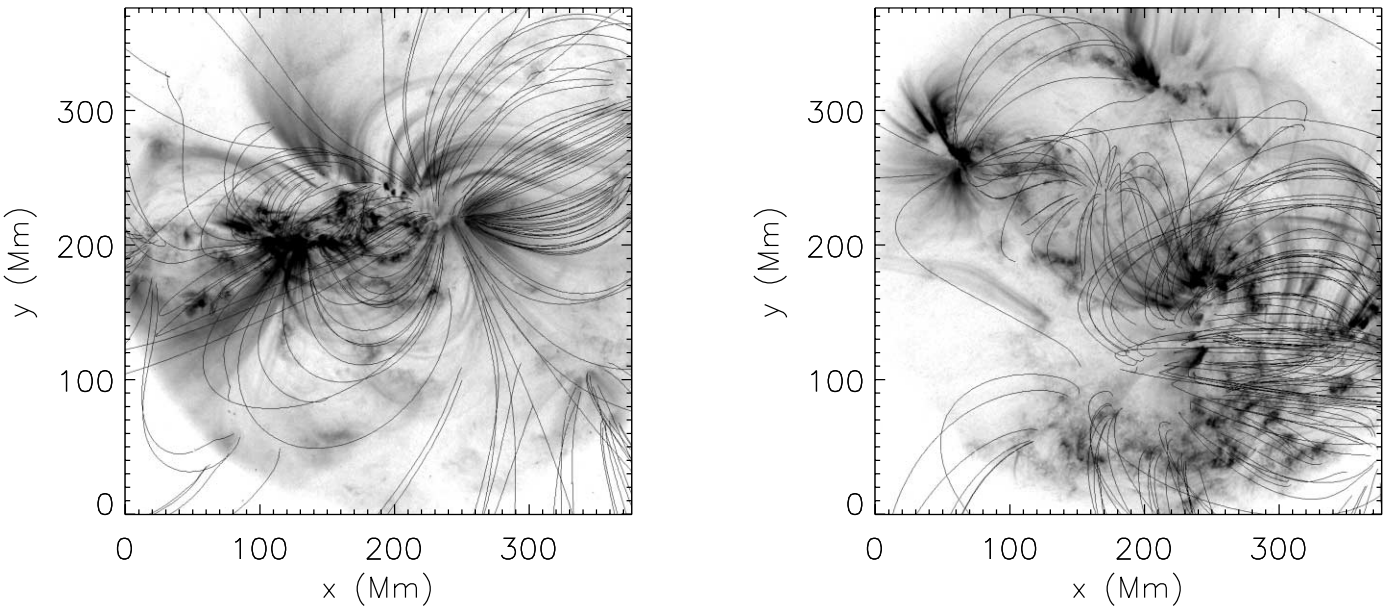


FIG. 4.—As Fig. 3, but for the significantly nonpotential cases 24 and 39 listed in Table 2. Color versions of such overlays for all cases studied here and a javascript animation are available in the electronic edition of the Journal.

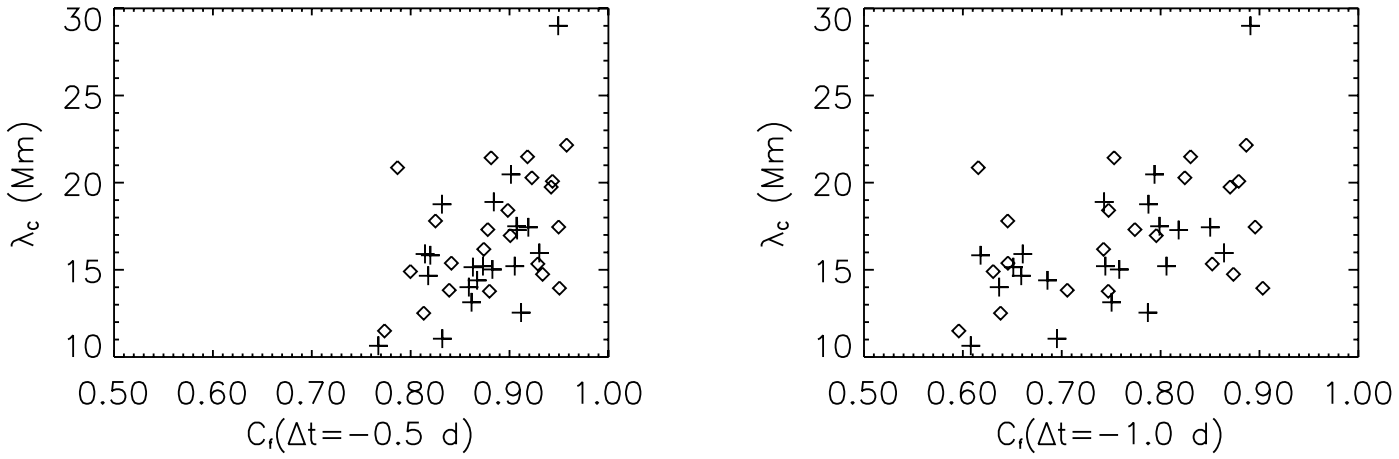


FIG. 5.—Spatiotemporal correlations for the magnetic fields: $C_f$ is the cross-correlation coefficient for the magnetogram at the time of the *TRACE* observation and that 0.5 (*left*) or 1.0 day (*right*) earlier; $\lambda_C$ is the *e*-folding distance of the average cross-correlation coefficient for shifts in the north-south and east-west directions. *Diamonds*: Near-potential cases; *plus signs*: nonpotential cases.

suggesting that we try measures that are biased toward such regions. We thus also compute spatiotemporal correlation measures for the magnetograms in which only fields exceeding absolute flux densities of 250 Mx cm$^{-2}$ are included, using either the fields as measured or the polarity patterns for the thresholded magnetograms. Neither yields a useful criterion for separation of near-potential and nonpotential coronal fields. Specifically, we compute $C_s$ defined as the cross-correlation coefficient for images of $B^*_+(x, y)$ and $-B^*_-(x, y)$, where subscript plus and minus signs indicate that only the positive or negative values are used, and the superscript asterisk indicates that all pixels with absolute values below the threshold of 250 Mx cm$^{-2}$ were zeroed. Figure 6 plots the temporal correlation coefficient for 0.5 and 1.0 day lags versus the distance at which $C_s$ peaks. Figure 7 shows a similar diagram in which only the polarity of the strong fields is used; i.e., $C_p$ is defined as the cross-correlation coefficient for two logical masks showing where $B_+(x, y)$ and $-B_-(x, y)$ exceed the threshold of 250 Mx cm$^{-2}$, respectively. The two categories of active regions are not significantly separated in these diagrams, from which we conclude that no simple large-scale spatial or temporal correlation property of the active regions unambiguously separates near-potential from nonpotential regions, regardless of whether we compute these measures for the entire regions or focus on high flux density regions.

### 4.2. *Flaring Properties*

The electrical currents leading to nonpotential coronae may be (part of) the currents that are involved in flaring activity. To study that, we investigate the flare properties of the two classes of active regions. We select a window ranging from 2 days prior to the time of the comparison of the *TRACE* observation with the model potential field to 1 day after that time. This choice is based on our finding, discussed in § 4.4, that the currents disappear on a timescale of typically 10–30 hr and often require about a day to build up to significant levels during flux emergence.

The flare listings in Tables 1 and 2 reveal a significant difference in the flaring properties of the samples: there are 2.4 times as many flares of class C or brighter in the nonpotential sample than in the near-potential sample: there are 0.0 X, 0.1 M, and 0.6 C class flares per day during the 3 day intervals for the near-potential cases in Table 1, in contrast to 0.1 X, 0.3 M, and 1.3 C class flares per day for the nonpotential entries in Table 2. Moreover, the nonpotential cases exhibit a less steep peak brightness distribution (Fig. 8) than either the near-potential cases or the overall sample of all flares listed in the NOAA

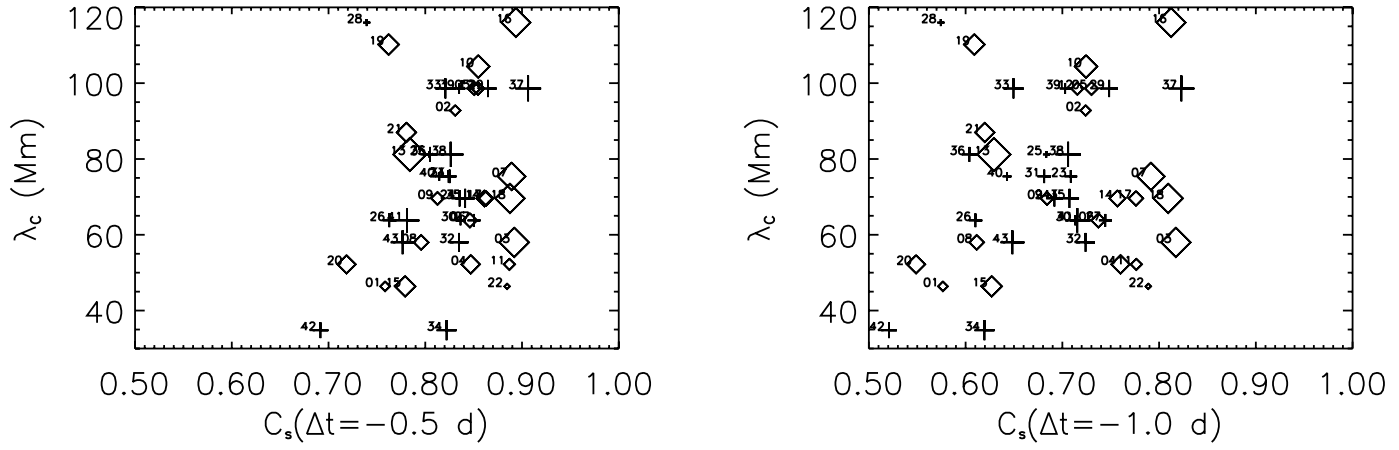


FIG. 6.—Spatiotemporal correlations for the strong-field regions. $C_s$ is the cross-correlation coefficient for the magnetogram at the time of the *TRACE* observation and that 0.5 (*left*) or 1.0 day (*right*) earlier, but for which all pixels with absolute flux densities below 250 Mx cm$^{-2}$ were masked out. Symbols as in Fig. 5, labeled by the case numbers as in Tables 1 and 2. Symbol size scales with the peak value of $C_s$.

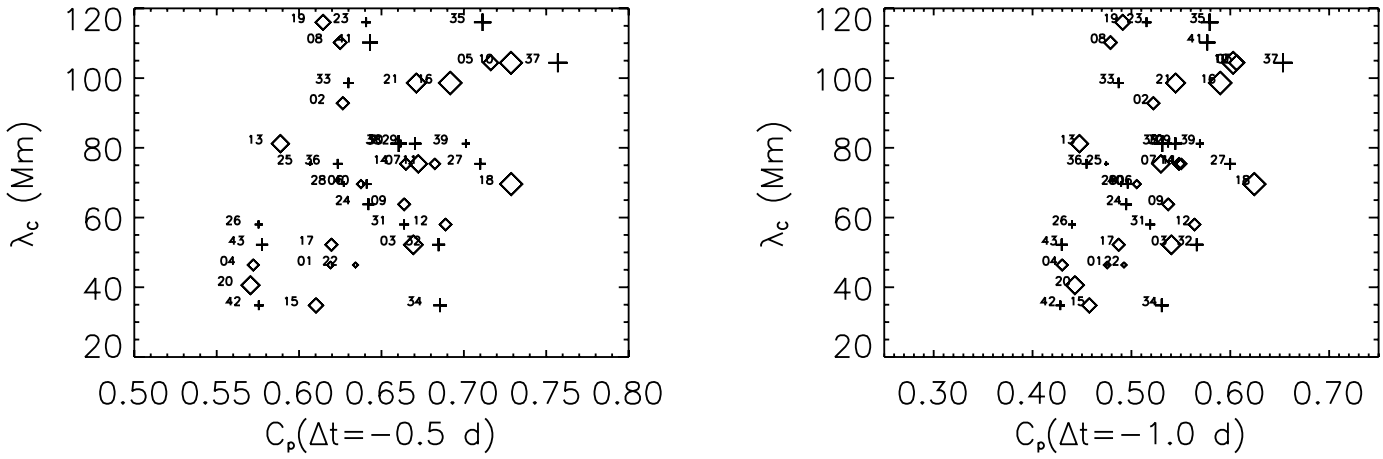


FIG. 7.—Spatiotemporal correlations for the polarity maps for strong-field regions. $C_p$ is the cross-correlation coefficient for the magnetogram at the time of the *TRACE* observation and that 0.5 (*left*) or 1.0 day (*right*) earlier, with all pixels with absolute flux densities below 250 Mx cm$^{-2}$ masked out and all remaining pixels set to $\pm 1$, depending on the field polarity; $\lambda_C$ and symbols as in Fig. 5. Symbol size scales with the peak value of $C_p$.

archives from 1999 April 1 through 2001 April 1 for which active-region sources were specified (i.e., applying the same selection criterion as for the flares tabulated in Tables 1 and 2).

We realize that for regions with many large flares, the smaller flares may not all be listed, or even be identifiable in the X-ray light curves. This may result in a somewhat reduced slope for the flare-energy distribution, but the distinction between the spectra is large enough that we believe the differences to be significant, as quantified by the reduced $\chi^2_\nu$ value of 2.4 in the comparison of the near-potential and nonpotential cases (assuming Poisson statistics to estimate uncertainties).

This difference in the spectral shape for the flare peak brightness results in an average peak brightness for X-ray flares that is 3.3 times higher for the nonpotential cases than for the near-potential ones, corresponding to an average brightness of M1.6 for the sample of nonpotential cases, compared to C4.8 for the near-potential cases and C5.4 for the general flare population. The combination of higher flare frequency and larger average flare brightness causes the flare-energy budget for the nonpotential cases to be at least an order of magnitude larger for the near-potential cases within the selected 3 day time intervals (a complete comparison should also reflect that flare durations tend to increase with peak brightness).

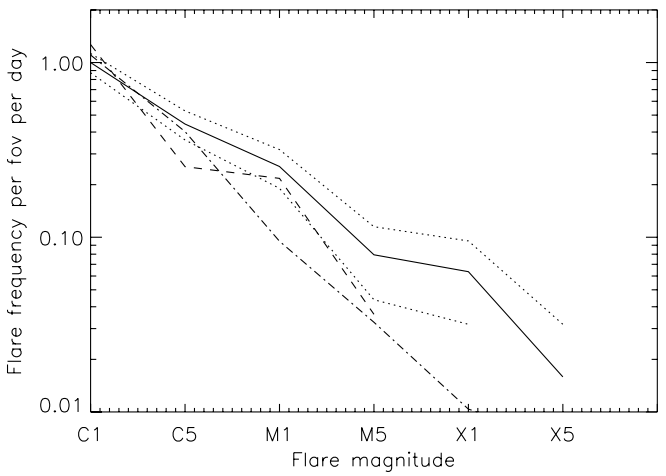


FIG. 8.—Flare frequencies per *TRACE* field of view per day for nonpotential regions (*solid lines*, with dotted lines showing the formal uncertainty interval assuming Gaussian statistics) and for near-potential regions (*dashed lines*, raised by a factor of 2.4). The dashed-dotted line shows the distribution of flare classes with identified active regions in the NOAA listings from 1999 April 1 through 2001 April 1. The latter are normalized to the nonpotential region's flare frequency for C2–3 flares to enable direct comparison of the spectral shapes.

Our finding that flare-energy spectra depend on some property of the active region samples is to be compared to the finding by Wheatland (2000b) that such spectra for individual regions are not significantly different from the overall set. It may be that his sampling for individual regions resulted in such low-number statistics that his tests did not show any differences as significant. We hypothesize, however, that the similarity of individual and population flare-energy spectra found by Wheatland holds when sampling over a substantial part of the lifetime of active regions, i.e., over the more impulsive initial phases as well as the more quiescent later phases. Conversely, our sampling differentiates between these phases.

Whereas the flare frequency and mean flare brightness are higher in the sample of nonpotential regions compared to the sample of near-potential ones, neither measure is useful as an unambiguous characteristic of the instantaneous degree of potentiality of the coronal field of individual regions. In fact, if the occurrence of flares in the 3 day window is used as a test for potential and nonpotential coronal fields, only 65% of the regions are correctly identified (see Table 1), which is only 15% better than a random selection.

It is not surprising that flare frequency or magnitude do not unambiguously differentiate between potential and nonpotential cases. On the one hand, flares are instabilities that may occur only after a substantial wait time, and the magnitude of the relaxation is not a direct measure for the available free energy in the field. Moreover, in order to raise any differences in behavior to a significant level, a fair number of flares needs to be observed for each region; a 3 day window is adequate to do that for the full sample of regions, but flare frequencies are too low to do that for each of the regions individually. For example, three of the nonpotential regions did not flare at all within the 3 day window.

On the other hand, flares likely remove or redirect coronal electrical currents, so, if there is a substantial interval between flares and the *TRACE* coronal images, the field may have relaxed to a near-potential configuration by the time the field lines are compared to the observed loops. Alternatively, growing regions may not have built up enough nonpotentiality yet to be observable

if the flares occur some time after the coronal field observation. This is likely why only 12 (55%) of the near-potential cases flared at least once within the time window. Of these 12 cases, only four exhibit flaring within the 10 hr immediately prior to the *TRACE* observation (cases 7, 10, 11, and 19), two between 10 and 18 hr (cases 6 and 14), and six show no flares in the 24 hr leading up to the *TRACE* observation (cases 1, 5, 8, 9, 12, and 21; the ambiguous case 45 also falls into this category).

### 4.3. *Filament Configurations*

Electrical currents are clearly involved in flares, and the enhanced flare frequency and brightness in nonpotential regions suggests that we explore another property of active regions known to involve large-scale current systems, namely, filaments over neutral zones. Whereas the magnitudes of currents in filaments are hard to derive from observations, the presence, size, and shape of filaments is readily inferred from H$\alpha$ observations. We have identified the full-disk H$\alpha$ images taken at Big Bear Solar Observatory nearest in time to the *TRACE* pointing on the same day. A comparison of cutouts from these H$\alpha$ images that roughly match the *TRACE* fields of view are shown in the electronic version of the Journal.

We find no clear differentiation between the two categories of fields: most of the fields of view have one or more filaments within the active region(s) or in the immediate vicinity, while the shapes or sizes of these filaments do not exhibit a clear correlation with the overall degree of potentiality of the coronal field. We hypothesize that compact and rapidly evolving currents such as those that drive flaring activity are more important to the overall coronal field geometry than the large-scale, slowly evolving, and perhaps much weaker currents in the filament configurations.

### 4.4. *Evolution of the Magnetic Field*

Inspection of magnetogram sequences over 3 day periods prior to the selected *TRACE* images results in a high degree of success in the separation of the two categories. Visual differentiations have a success rate of about 70% if based on the following qualitative criteria, increasing up to 88% if a quantiative threshold for the flux involved is set (as discussed below). Nonpotentiality of the active-region coronal field can be expected when

*Criterion A.*—(71% of all nonpotential cases) the field is still emerging, or was within the last day, with meandering or fragmented polarity separation lines, associated with sustained shearing motions of the field as it sorts itself out; in some cases this leads to nonpotential fields low down while leaving the largest scales nearly potential;

*Criterion B.*—(43%) there are touching and rapidly evolving (canceling) opposite-polarity concentrations of high flux density up to $\sim$30 hr earlier, unless that is a small part of the overall flux in the region; if these form a relatively small and compact fraction of the overall active region, the nonpotentiality is weak or limited to that compact region; or

*Criterion C.*—(14%) the field emerges within or adjacent to an existing configuration, provided it introduces significant new flux, and does not have a neutral line shared with that of the preexisting field.

Several regions fall into two or three of the above categories, causing the total to add up to 128%.

In contrast, the (near-) potentiality of the overlying field is not (necessarily) affected when

*Criterion D.*—(41% of all near-potential cases) strong mixed-polarity emergence has strongly decreased in the last 10–20 hr, or when such emergence is just starting;

*Criterion E.*—(36%) the configuration is that of a simple, gradually evolving bipole;

*Criterion F.*—(18%) flux cancels rapidly in a mature or decaying region having a simple bipolar configuration with a relatively straight and well-defined polarity inversion line or

*Criterion G.*—(5%) relatively small bipoles emerge within an existing active region, regardless of their position relative to the neutral line.

With the above criteria, visual inspection of the magnetogram sequences successfully characterizes the (non) potentiality of the coronal field for 30 (70%) of the 43 cases in Tables 1 and 2.

Not surprisingly, the above differentiating criteria need to be met by a substantial fraction of the overall flux, as is illustrated by, e.g., near-potential cases 2, 5, 8, 11, 13, and 16 where they are met only in small regions involving relatively little flux. On the other hand, it clearly does not need to involve a majority fraction of the total flux in the region, as can be seen, for example, in the nonpotential case 27 (within the area circled in Fig. 2). We have used the magnetogram sequences to identify the fluxes involved in the processes A–C described above; the total absolute fluxes involved in these processes and in the active regions within the fields of view are then measured on the magnetogram nearest in time to the entries in Tables 1 and 2. The total absolute fluxes for the near-potential and nonpotential cases are not significantly different at $(28 \pm 16) \times 10^{21}$ and $(32 \pm 20) \times 10^{21}$ Mx, respectively, where the uncertainties indicate the standard deviation in the samples. The average flux involved in processes A–C for the nonpotential cases amounts to $(9 \pm 5) \times 10^{21}$ Mx within a 48 hr period prior to the times in Table 2, or 31% $\pm$ 13% of the total flux (see the next-to-last column of Table 2). The estimated maximum flux that meets criteria D–G for the near-potential cases is $(2.6 \pm 2.0) \times 10^{21}$ Mx within a 48 hr period prior to the times in Table 1, or 8% $\pm$ 4% of the total flux (see the next-to-last column of Table 1). Of all the nonpotential cases (excluding those for which the flux estimates are rather uncertain), only one involves less than 15% of the flux, and of all the near-potential cases only one involves more than that fraction. Using a cutoff of 15% of the total flux in addition to the above qualitative criteria correctly identifies 89% of the cases, including those with uncertain flux values (see Table 4).

There is a significant latency in the coronal response to the photospheric driver. On the one hand, we find that the nonpotentiality of the active-region coronae persists for some time after criteria A–C cease to be met. Specifically, we find that the criteria A–C were no longer met at the time of the evaluation of the corona nonpotentiality for six of the nonpotential regions. The times that had elapsed since these criteria were last met are as follows: $\approx$6 hr for case 29 (ending in the top right of the circle in Fig. 2, and earlier also on the left-hand edge), a few hours for case 32 (near the center of the circle in Fig. 2), $\approx$16 hr for case 38 (circled), $\approx$22 hr for case 39 (circled), and $\approx$36 hr for case 43. Similarly, three of the regions classified as near-potential met the criteria A–C some time prior to the time at which they were classified: $\approx$24 hr for case 7, $\approx$8 hr for case 10, and $\approx$22 hr for case 19. We therefore conclude that most of the current leading to an overall nonpotentiality of active-region coronae disappears typically $\tau = 19 \pm 9$ hr after criteria A–C cease to be met; the value of $\tau$ for individual cases can differ from the sample mean by about a factor of 2.

Some latency may also exist when nonpotentiality is building up. For example, once an adequate fraction of the active-region flux meets the criteria for a nonpotential coronal field, that nonpotentiality is found to propagate into the corona within $\approx$8 hr

TABLE 4
Active-Region Coronae Classification Percentages

| Poteniality (1) | Actual (2) | Nonflaring (3) | Flaring (4) | $<f$ (5) | $>f$ (6) |
|---|---|---|---|---|---|
| Near..... | 51% | 22% | 28% | 49% | 2% |
| Non..... | 49% | 7% | 42% | 9% | 40% |

Note.—Percentages of active-region coronae that are unambibuously classified as near-potential or nonpotential (Tables 1 and 2, respectively) and (1) that are either flaring or nonflaring (C-class or larger) (cols. [3] and [4]), or (2) that meet qualitative diagnostics A–G (§ 4.4) within a 3 day interval with less or more than $f = 15\%$ of the total flux (cols. [5] and [6], respectively).

for case 41. In cases 3 and 6, in contrast, mixed-polarity flux emergence suggests the formation of nonpotential fields shortly after the selected EUV observation, but no clear indications of nonpotentiality in the coronal field are seen within the subsequent 18 hr (after which *TRACE* switched targets).

We note that the nonpotentiality of the corona over three regions remains unexplained. In case 25, the magnetogram sequence shows no obvious patterns to differentiate it from the near-potential cases, nor does the substantial filament within the region appear unprecedented in the near-potential cases (e.g., 6, 9, 19, or 22). In case 32, the fragmentation and apparent mild rotation of the spotgroup is the only unusual feature. Case 41 is unusual in that a neighboring (trailing) emerging region clearly meets criteria A and B, and that region connects to the trailing part of the central region AR 9240, thus potentially deforming much of its corona. There is only one other region, case 23, in which the proximity of a distinct neighboring active region significantly influences the (non) potentiality of the coronal field by interaction shortly after emergence (circled in Fig. 2).

Table 3 lists four regions in which the classification by three of the authors as near-potential or nonpotential was not unanimous. Cases 44 and 46 were classified as near-potential by two out of the three assessments, while cases 45 and 47 were classified as nonpotential by two out of the three assessments. All of these cases meet one or more of criteria A–C for fractions of the total flux ranging from $\sim$7% to $\sim$20%. These flux fractions are near the 15% threshold discussed above, which may explain the ambiguous assessments of their (non) potentiality.

## 5. CONCLUSIONS

Our study suggests that time series of line-of-sight magnetograms spanning approximately 48 hr at a cadence on the order of an hour can be used to identify active regions that carry electrical currents that cause significant nonpotentiality in their coronal fields that likely affects its coupling to the larger-scale coronal, or possibly even heliospheric, magnetic field. These time series can be used to identify the rapidly evolving mixed polarities with unusual dynamics that we find to be associated with such current systems.

We conclude that significant nonpotentiality of the overall active-region coronal field is mostly driven by sufficiently complex and large flux emergence within the active region itself within $\sim$10–30 hr prior to the observation of the coronal configuration. We have found no correlation measures based on entire active regions that are helpful in the separation of near-potential from nonpotential cases (compare the search for flaring diagnostics by, e.g., Leka & Barnes 2003). However, subjective signatures can be found in magnetogram sequences of up to 2 days prior to the coronal observation: time sequences of magnetograms can be used to separate near-potential from nonpotential active-region coronae with a success rate of at least $\approx$70%. By selecting regions in which at least 15% of the region's flux is involved in these signatures (A–C in § 4.4) the success rate increases to $\approx$90%. Both these magnetogram signatures and the (non) potentiality of the coronal field are useful indicators for the flare frequency and flare magnitude of active regions.

We find that the coronal field over active regions is likely significantly nonpotential if more than 15% of the region's flux is involved in (1) flux emergence with meandering or fragmented polarity separation lines, often associated with significant shearing motions of the field, or (2) substantial rapidly evolving, opposite-polarity concentrations which are in contact at a resolution of 4″ (consistent with most of the "evolutionary changes" identified as common preflare conditions in the thorough review by Martin 1980). The potentiality of the coronal field is not significantly affected when relatively small bipoles emerge within an existing active region or when there is rapid flux cancellation in mature regions with a simple bipolar organization and a well-defined, smooth polarity inversion line. The presence and shape of filaments within or near the active regions do not appear to be indicative of the degree of coronal nonpotentiality: the slowly evolving, large-scale current systems in the filaments are apparently less important to the (non) potentiality of the active region coronae than the current systems emerging with, or induced by, emerging flux systems that are often involved in flaring activity.

Flares and eruptions tend to be more frequent and larger in nonpotential regions. Impulsive activity also occurs in active regions with nearly potential large-scale coronal fields but is observed in 19% of the near-potential cases (4 of 21) within 10 hr of the corona-field comparison, in 29% of the cases within 18 hr, and 43% within 48 hr prior to the observation. This increasing fraction of flare-generating regions with increasing time interval between flaring and the comparison of loops and field lines supports our hypothesis that the current systems that drive the nonpotentiality of the coronal field are not long lived: based on the present sample, we estimate a characteristic lifetime on the order of 20 hr. That value is consistent with the observed decay timescale of 27 hr for patches in active regions where significant currents thread the photosphere (Pevtsov et al. 1994; Burnette et al. 2004). It thus appears that the currents that cause the nonpotentiality of the coronal active-region field (mostly) penetrate the photosphere and that these have a lifetime on the order of 1 day, unless sustained by the ongoing emergence of current-carrying or current-inducing new flux.

Cases that were misidentified using the above criteria may have had an unusually long decay time of the electrical currents, or perhaps the currents associated with emerging flux need not necessarily lead to an appreciable reorientation of the coronal magnetic field. One possibility is that the alignment of the existing and newly emerging magnetic fields need not necessarily be so incompatible that nonpotentiality or destabilization occurs as the fields adjust to each other.

The properties of emerging flux that induce nonpotentiality of the overall active-region corona are clearly related to the flare potential of the region. The latter, in turn, has been suggested to be related to helicity buildup. Our study indirectly suggests that any such helicity buildup is likely related to flux emergence within a $\sim$20 hr period before the coronal observation, consistent with the conclusions reached by Wheatland (2000a) and by Démoulin et al. (2002a, 2002b) for the study of AR 7978.

In apparent contrast to our findings, Moon et al. (2002) and Yang et al. (2004), for example, conclude that horizontal shear flows are responsible for the flaring behavior of AR 8100 and

AR 10486, respectively. But upon inspection of the evolution of the magnetic field in these regions[3] during the days prior to the times used in the above studies, we find signs of flux emergence matching our criteria A and B: AR 8100 shows substantial emerging flux in the second half of 1997 November 2, i.e., some 30 hr before the data set studied by Moon et al. (2002), with significant emergence ending only hours before their observations, while in AR 10486 substantial flux emergence with opposite polarities in close proximity and apparent shearing motion is sustained for multiple days. In general, therefore, we concur with the findings of Wheatland (2000a) and Démoulin et al. (2002a, 2002b): emergence of currents and associated helicity with magnetic flux into preexisting active-region field configurations appears to be required to drive active-region flaring and—as we find here—coronal nonpotentiality.

Shear flows have been suggested to be responsible for flaring activity (e.g., Harvey & Harvey 1976; Henoux & Somov 1987; Moon et al. 2002), but we find that they do not by themselves drive enhanced flaring or coronal nonpotentiality: our present sample demonstrates that these properties related to coronal free energy require appropriately complex and dynamic flux emergence within the preceding $\sim$30 hr.

In a study that focused on flare-generating active regions, Wheatland (2000a) concluded that the free energy in active-region fields available for flaring activity is not built up by persistent stressing of the surface field, but instead emerges with the field from below the photosphere. His reasoning follows an argument made earlier by Melrose (1991): if field stressing by surface flows were responsible for the buildup of free energy, then the induced upward and downward currents within a polarity region of the magnetic field should balance. Whereas the signed currents are indeed found to balance over entire active regions to within the uncertainties, Wheatland found that the upward and downward currents within a given polarity commonly do not balance and hence must be introduced by flux emergence.

Following Melrose (1991), Wheatland (2000a) argues that the long inductive timescales of extended, large current systems preclude significant changes in the magnitude of the currents on the short timescales of flares, and that therefore currents are redirected rather than substantially modified in magnitude. Our present study suggests that these electrical currents in fact decrease, annihilate, or redirect markedly on a timescale on the order of 1 day, because the nonpotentiality of the entire active-region corona disappears within typically a day after the flux emergence ceases. Interestingly, such current decreases do not appear to contribute significantly to the overall quiescent coronal heating (e.g., Metcalf et al. 1994; Fisher et al. 1998) but appear instead related to flare processes (which may dissipate, cancel, or expel such currents).

Finally, we address the consequences of the evolution of active-region electrical currents for heliospheric modeling: (1) how many active regions are typically clearly nonpotential at any given time, and (2) how does that affect the PFSS modeling?

[3] See the electronic version of the Journal.

The first question is most readily addressed. Our study shows that nonpotentiality of the active-region corona and flaring activity are strongly related, showing that the large majority of flares occur in nonpotential regions. That enables us to estimate the characteristic timescale over which active regions sustain their nonpotentiality. In the 2 year cycle-maximum interval from 1999 April 1 through 2001 April 1, the NOAA event logs list 2220 flares for 898 active regions for which an active region was assigned (out of 4306 flares overall), or 2.5 flares per identified region per day of class C or larger. Our sample of nonpotential regions exhibits 1.9 such flares per region per day. Hence, the nonpotentiality of active regions should be sustained typically for 1.3 days. The average lifetime of active regions is hard to estimate, as the decay process involves a smooth transition from a mature, coherent active region to enhanced network. Using the data compiled by Harvey (1993), her Table 2 and Fig. 1*a*, the average lifetime is 4.2 days. Significant nonpotentiality of active regions occurs mostly in relative large, and thus long-lived, active regions. The above statistics thus suggest that nonpotentiality is sustained for less than 30% of their lifetime. The definition of a lifetime for active regions is clearly subjective, and the above value is perhaps unduly short as this average is dominated by the high frequency of smaller, shorter-lived regions. At the other extreme, the lifetime of flux patterns on the solar photosphere around cycle maximum has been estimated to be as long as 4 months (Schrijver & Harvey 1994), of which only $\approx$1% is likely spent carrying significant electrical currents.

How does that affect the potential-field source-surface (PFSS) modeling? If indeed active-region flux patterns in the solar photosphere spend only $\approx$1% of their lifetime carrying significant electrical currents, then only a small fraction of the solar corona carries strong electrical currents whose effects do not cancel on large scales at any given time. That is consistent with the overall success of the PFSS model in representing the large-scale coronal field as mapped by, e.g., quiescent wind streams or coronal-hole boundaries. However, Schrijver & DeRosa (2003) argue that around cycle maximum, some 30%–50% of the interplanetary magnetic field maps directly onto mature active regions, of which—as we suggest here—up to 30% is poorly approximated by a potential field. These findings together suggests that $\approx$10% of the flux in the IMF at cycle maximum differs significantly from the PFSS model assumptions and that consequently some of the mapping of field lines and the inferred field expansion (which determines wind speeds) may be substantially in error. On the other hand, we conclude that most of the solar photospheric flux is compatible with the PFSS model assumptions most of the time.

We thank the referee for suggesting that we be more quantitative in formulating the results. This work was supported by NASA/LWS grant NAG5-10832, *TRACE* contract NAS5-38099 with NASA Goddard Space Flight Center, MDI-SOI contract NAS5-30386 with NASA through Stanford contract PR 9162, and Lockheed Martin Independent Research funds.

REFERENCES

Burnette, A. B., Canfield, R. C., & Pevtsov, A. A. 2004, ApJ, 606, 565
Démoulin, P., Mandrini, C. H., Van Driel-Gesztelyi, L., Lopez Fuentes, M. C., & Aulanier, G. 2002a, Sol. Phys., 207, 87
Démoulin, P., Mandrini, C. H., van Driel-Gesztelyi, L., Thompson, B. J., Plunkett, S., Kovári, Z., Aulanier, G., & Young, A. 2002b, A&A, 382, 650
Fisher, G., Longcope, D., Metcalf, T., & Pevtsov, A. 1998, ApJ, 508, 885
Handy, B. N., et al. 1999, Sol. Phys., 187, 229
Harvey, K. L. 1993, Ph.D. thesis, Utrecht Univ.
Harvey, K. L., & Harvey, J. W. 1976, Sol. Phys., 47, 233
Henoux, J. C., & Somov, B. V. 1987, A&A, 185, 306

Hoeksema, J. T. 1984, Ph.D. thesis, Stanford Univ.
Leka, K. D., & Barnes, G. 2003, ApJ, 595, 1296
Leka, K. D., Canfield, R. C., McClymont, A. N., & van Driel-Gesztelyi, L. 1996, ApJ, 462, 547
Martin, S. F. 1980, Sol. Phys., 68, 217
Melrose, D. B. 1991, ApJ, 381, 306
Metcalf, T. R., Canfield, R. C., Hudson, H. S., Mickey, D. L., Wülser, J.-P., Martens, P. C. H., & Tsuneta, S. 1994, ApJ, 428, 860
Moon, Y.-J., Chae, J., Choe, G. S., Wang, H., Park, Y. D., Yun, H. S., Yurchyshyn, V., & Goode, P. R. 2002, ApJ, 574, 1066
Neugebauer, M., et al. 1998, J. Geophys. Res., 103, 14587
Pevtsov, A. A., Canfield, R. C., & Metcalf, T. R. 1994, ApJ, 425, L117
Schatten, K. H., Wilcox, J. M., & Ness, N. F. 1969, Sol. Phys., 6, 442
Scherrer, P. H., et al. 1995, Sol. Phys., 162, 129
Schrijver, C. J., & DeRosa, M. L. 2003, Sol. Phys., 212, 165
Schrijver, C. J., & Harvey, K. L. 1994, Sol. Phys., 150, 1
Wang, Y.-M., & Sheeley, N. R. 1992, ApJ, 392, 310
Wheatland, M. S. 2000a, ApJ, 532, 616
———. 2000b, ApJ, 532, 1209
Yang, G., Xu, Y., Cao, W., Wang, H., Denker, C., & Rimmele, T. R. 2004, ApJ, 617, L151
Zhao, X., & Hoeksema, J. T. 1995, Adv. Space Res., 16, 181